Experimental design and stochastic modeling of hydrodynamic wave propagation within cavities for wind tunnel acoustic measurements

van Dercreek, Colin; Amiri-Simkooei, Alireza; Snellen, Mirjam; Ragni, Daniele

DOI
10.1177/1475472X19889949

Publication date
2019

Document Version
Final published version

Published in
International Journal of Aeroacoustics

Citation (APA)
van Dercreek, C., Amiri-Simkooei, A., Snellen, M., & Ragni, D. (2019). Experimental design and stochastic modeling of hydrodynamic wave propagation within cavities for wind tunnel acoustic measurements. *International Journal of Aeroacoustics*, *18*(8), 752-779. https://doi.org/10.1177/1475472X19889949

Article

aeroacoustics

International Journal of Aeroacoustics
2019, Vol. 18(8) 752–779

DOI: 10.1177/1475472X19889949
journals.sagepub.com/home/jae
SAGE

Experimental design and stochastic modeling of hydrodynamic wave propagation within cavities for wind tunnel acoustic measurements

Colin P VanDercreek[1], Alireza Amiri-Simkooei[1], Mirjam Snellen[1] and Daniele Ragni[2]

Abstract

This study investigates how embedding microphones in different cavity geometries along the wall of a wind tunnel reduces the measured turbulent boundary layer pressure fluctuations. The effect of these cavities on the measured signal-to-noise ratio of an acoustic source with flow present was also quantified. Twelve cavity geometries defined by their depths, diameters, chamfer, opening percentage, and mesh covering were tested. The cavity geometries were selected using a design of experiments methodology. The application of design of experiments enabled a statistically sound and efficient test campaign. This was done by applying a D-optimal selection criterion to all potential cavity geometries in order to select 12 cavities to allow for the individual effect of the geometric parameters such as depth and diameter to be quantified with statistical confidence. The resulting wind tunnel test data were fit to a generalized additive model. This approach quantified the relative effect of these parameters on the turbulent boundary layer pressure spectral energy and signal-to-noise ratio while accounting for non-linear frequency dependence. This experimental investigation quantified how much increasing depth reduces the turbulent boundary layer spectral energy and increases signal-to-noise ratio. It also

---

[1]Section Aircraft Noise and Climate Effects (ANCE), Faculty of Aerospace Engineering, Delft University of Technology, Delft, The Netherlands
[2]Section Aerodynamics, Wind Energy, Flight Performance and Propulsion (AWEP), Faculty of Aerospace Engineering, Delft University of Technology, Delft, The Netherlands

Corresponding author:
Colin P VanDercreek, Section Aircraft Noise and Climate Effects (ANCE), Faculty of Aerospace Engineering, Delft University of Technology, Delft, The Netherlands.
Email: c.p.vandercreek-1@tudelft.nl

showed that a mesh covering reduces the boundary layer noise by 8 dB. It was also quantified how much reducing the cavity area from the opening of the cavity to the base of the microphone reduces the measured boundary layer spectral energy. Additionally, the model quantified the interactions between the mesh and cavity area as well as the change in area.

Keywords
Beamforming, cavity acoustics, design of experiments, generalized additive model

Date received: 9 April 2019; Revised 19 July 2019; accepted: 25 July 2019

Introduction

Acoustic arrays are frequently used with beamforming algorithms in wind tunnels to localize and quantify acoustic noise within a region of interest. These techniques are successfully used for aeroacoustic measurements[1] of conventional airfoils whose trailing edge noise is approximately 60 dB/m depending on the flow conditions.[2] However, as the sound generation characteristics of airfoils are modified such that the radiated noise levels become lower by incorporating features such as trailing edge serrations,[3] it is important to optimize acoustic measurement techniques for these lower levels. These measurements in closed test section wind tunnels can be hindered by turbulent boundary layer (TBL) noise generated by the wind tunnel wall along with other acoustic noise sources.[1] These fluctuations create a lower bound below which acoustic measurements are not feasible. This is due to the acoustic signal energy level generated by the test article being overwhelmed by the higher background noise.[4] Therefore, this noise needs to be mitigated to enable effective aeroacoustic measurements of low intensity sources.

Signal processing and recessing cavities are two approaches to reducing TBL noise and increasing signal-to-noise ratio (SNR). TBL noise is generated from the incoherent pressure fluctuations in the viscous and logarithmic regions of the boundary layer,[5] which signal processing techniques can remove from the acoustic signal. For example, one method to achieve this is by removing the diagonal of the beamforming covariance matrix[6–8] which can reduce the measured background noise by approximately 25 dB at 5 kHz for a tunnel Mach number of 0.22.[4] However, it is advantageous to couple these signal processing techniques with actual reductions in the TBL hydrodynamic fluctuations to improve the SNR of acoustic beamforming arrays. Recessing microphones in cavities and covering these cavities with a metallic mesh or Kevlar[4,9,10] is a common approach for reducing TBL wall noise. These approaches, coupled with signal processing, can reduce the measured background noise approximately by an additional 10 dB for an array.[4] This results in a typical improvement in SNR by 5 dB. The focus of this study is to evaluate how cavity geometries attenuate the impingement of boundary layer hydrodynamic pressure fluctuations on a microphone and the resulting improvement to SNR.

An experiment was designed to study the influence of cavity geometry on two response variables: the amount of the spectral energy due to the TBL pressure fluctuations and the SNR with respect to a broadband acoustic source. This experiment used a design of experiments (DOE) methodology to select the number of cavities and their geometry. DOE is a statistical tool for test planning that ensures randomization while covering a broad range of the design space of interest. The primary advantage of DOE over the more traditional one-factor-at-a-time (OFAT) approach to testing is that it reduces required test resources by making more efficient use of the potential experimental design space while providing insight into how different factors interact with each other.[11] The resulting test matrix ensures a sufficient number of runs to quantify the influence of different factors with statistical confidence. The resulting data are used to develop a stochastic model to determine which parameters have the most influence on the response variables. In this experiment the following geometric parameters were systematically varied: depth, opening area, mesh, and change in area with depth. The wind tunnel speed was varied to determine how different designs perform at different wind speeds. The presence of a broadband noise source was used to calculate the SNR of the cavities when measuring a source of interest. Two generalized additive models (GAMs) with mixed effects were developed to quantify the relationship between different geometries and the TBL energy and SNR response variables.

This paper has two goals. The first goal is to introduce the novel application of DOE methodology to efficiently maximize the potential experimental space. The second goal is to describe the application of GAMs to identify and quantify the influence of geometric parameters and their mutual interactions on the response variables of interest, the propagation of TBL spectral energy within a cavity, and SNR. The long term application of this experimental data and resulting insights is to support future deterministic model development with the goal of optimizing cavity designs.

In the "Theoretical background" section, the equations treating cavity depth and mesh are treated. In the "Experimental set-up" section, the details of the experiments are provided. The "Experimental results" section summarizes the boundary layer hot-wire and pressure fluctuations measurements. The "Establishing an empirical model" section discusses the approach to developing the statistical models. The "Experimental results" section presents the results and analysis of the measured response variables. From this we established an empirical model in the "Model predictions" section. The last section provides the conclusions of this work.

Theoretical background

Cavity depth, area, change in area, and a mesh covering affect the measured boundary layer pressure spectra.[4,10] Increasing the cavity depth reduces the wall pressure fluctuations measured by the microphones due to the hydrodynamic and acoustic waves being cut-off within the cavity.[1] The area of the cavity along with the wave number of the wave determines whether or not a wave is cut-on.[12] Furthermore, changing the area along the direction of propagation results in transmission losses due to partial reflection of incoming waves.[12] The mesh further attenuates the hydrodynamic fluctuations while eliminating vortex shedding from the upstream edge of the cavity which can cause resonance within the cavity.[4]

The propagation of hydrodynamic waves from the boundary layer into the cavity can be modeled by with an expression in the form of equation (1)

$$P(z,r,\theta)=\sum_{m=\infty}^{\infty}\sum_{\mu=1}^{\infty}\left(A_{m\mu}e^{ik_{m\mu}z}+B_{m\mu}e^{-ik_{m\mu}z}\right)U_{m\mu}(r)e^{-im\theta} \tag{1}$$

This equation is the generalized solution for the pressure distribution within a cylindrical cavity. In this equation, z is the distance along the propagation path from the boundary layer, r is the radial position within the cavity, θ is the angular position, $k_{m\mu}$ is the axial wave number, $A_{m\mu}$ and $B_{m\mu}$ are the downstream and upstream modal coefficients, respectively.[12] The radial coefficients are represented by $U_{m\mu}$, where m and μ are the mode indexes. Equation (2) is the expression for the axial wave number, where ω is the angular frequency and $\alpha_{m\mu}$'s are the radial wave numbers

$$k^{\pm}_{m\mu} = \pm\sqrt{\omega^2 - \alpha_{m\mu}} \tag{2}$$

The radial wave numbers are the solutions to the first derivative of a Bessel function of the first kind, $J'_m(\alpha_{m\mu}a) = 0$, and are proportional to the cavity radius, a.[12] When $k_{m\mu}$ is imaginary, the mode is cut-off.

The reduction in spectral energy due to the cavity depth within equation (1) is represented by the expression $e^{ik_{m\mu}z}$. When the incident wave is cut-off, the axial wave number is imaginary and therefore the energy reduces exponentially with distance. For the cavity area, as seen in equation (2), the radius along with the axial wave number has a potential impact on the spectral energy within the cavity. Changing the cavity area along the propagation path results in the downstream modal coefficients, $A_{m\mu}$, to scatter.[12] This scattering results in energy being reflected in the upstream direction and therefore reduces the downstream propagating energy. The mesh attenuates the hydrodynamic pressure fluctuations. Thus, it significantly reduces the TBL spectral energy while only reducing the acoustic signal by approximately 2 dB.[4] This can be modeled as an impedance across the mesh as seen in equation (3). In this equation, Z_{mesh} is the impedance term, p_{below} is the pressure amplitude below the mesh, p_{above} is the pressure amplitude above the mesh, and v is the velocity across the mesh (Sijtsma, personal communication, 14 March 2018.)

$$Z_{mesh}(\omega) = \frac{p_{below} - p_{above}}{v} \tag{3}$$

These equations are primarily used to assist in the theoretical understanding of how the TBL noise is affected by the cavity. The model discussed in this work is empirical and is intended to be used to validate future cavity designs. Further discussion of developing a deterministic model applying this theory to cavity geometries is discussed in Vandercreek et al.[13]

Experimental set-up

The experimental campaign was designed to quantify the effect of the interaction between cavity geometries and boundary layer pressure fluctuations on two response variables. The response variables are the amplitude of the boundary layer hydrodynamic spectral energy measured at the base of the cavity and the resulting SNR of the acoustic source with respect to these TBL spectra. These data were collected with LinearX M51 and M53 microphones installed at the base of each cavity. Twelve cavity geometries were tested in the TU Delft Low speed Turbulence Tunnel (LTT) by mounting them flush on the tunnel floor. TBL spectral measurements were taken in an empty wind tunnel test section to minimize unwanted sources of noise. SNR measurements used an omnidirectional speaker mounted in the tunnel center line, 0.53 m above the cavities. In addition to the microphone measurements, the boundary layer along the tunnel wall was measured with hot-wire anemometry (HWA). HWA data were used to calculate boundary layer thickness (δ_{99}, δ_{θ}), the shape factor (H), and to estimate the friction velocity (u^{*}). These properties are used to normalize the pressure spectra of the boundary layer.[5,14] The boundary layer was not tripped and therefore it was varied by changing the tunnel speed. Measurements were taken at flow speeds of 30, 50, and 70 m/s.

The 12 cavities were analyzed in terms of the following geometric parameters: depth, opening area, mesh, and change in area with depth. For the manufacturing of the cavity, they were defined in terms of depth, diameter, mesh, opening percentage, and the 45° chamfer depth. For the subsequent analysis, the geometric parameters were defined in terms of opening area, depth, change in area, and presence of a mesh. The opening area is calculated from the diameter, the opening percentage, and the chamfer. The change in area is defined as the ratio between the area of the opening of the cavity and the bottom, which is therefore calculated from the chamfer, diameter, and opening percentage. The geometries, as machined, are shown in Table 1. Figure 1 illustrates the definition of these parameters. The diameter and depth of the cavities were chosen to avoid acoustic resonance within the frequency range of interest (250 Hz to 7 kHz). The lowest estimated acoustic eigenfrequency for all cavities was 12 kHz for cavity 5A which was modeled as a Helmholtz resonator. The stainless steel mesh was placed over the top of six cavities and was installed with epoxy. The mesh has a density of 200 threads/cm with a wire diameter of 0.025 mm. The 12 cavities, were machined into two aluminum plates, each consisting of six cavities and one flush mounted microphone. This was done to allow for multiple cavities to be tested simultaneously. Cross sections of both plates can be seen in Figure 2. The plates are 1 m wide and each cavity was spaced at least 120 mm apart to avoid span-wise coherence.[15,16]

Wind tunnel measurements

The experiment was conducted at the TU Delft LTT wind tunnel. The LTT is an atmospheric closed test section wind tunnel capable of air speeds up to 120 m/s. The test section is

Table 1. Twelve cavity geometries, Flush A and Flush B are the flush mounted microphones for each plate.

Designation	Diameter (mm)	Mesh	Depth (mm)	Opening (%)	Chamfer (mm)
1A	10.0	Yes	5.0	100	4.0
2A	10.0	Yes	10.0	100	0.0
3A	5.0	No	5.0	100	4.0
4A	5.0	No	5.0	50	0.0
5A	10.0	Yes	10.0	50	4.0
6A	10.0	No	5.0	100	0.0
Flush A	6.0	No	0.1	100	0.0
7B	5.0	No	10.0	50	0.0
8B	5.0	Yes	10.0	100	0.0
9B	10.0	No	10.0	50	0.0
10B	5.0	Yes	5.0	100	4.0
11B	10.0	Yes	10.0	50	4.0
12B	5.0	No	5.0	50	4.0
Flush B	2.7	No	1.0	100	0.0

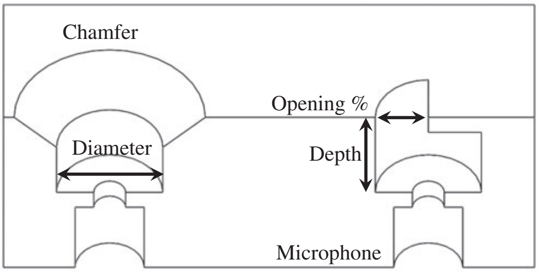

Figure 1. Cut away illustration of the cavity geometric parameters, mesh covering not pictured.

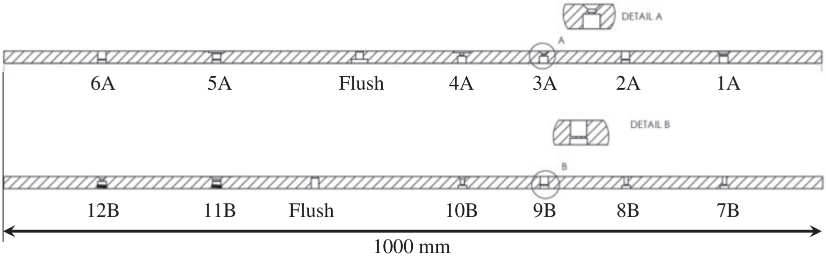

Figure 2. Cross sectional view of the plates containing the cavities under test.

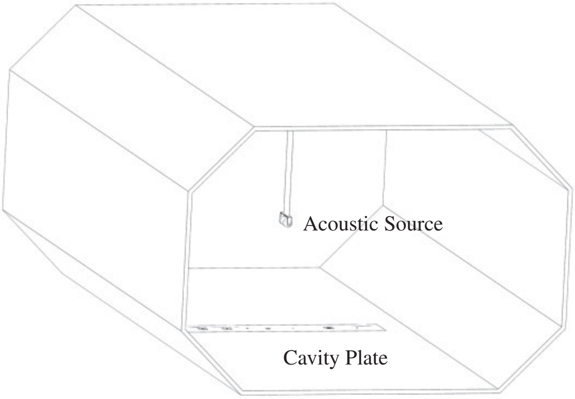

Figure 3. LTT test section with acoustic source and cavity plate installed.

1.8 m wide by 1.25 m tall. Free-stream turbulence is 0.015% with smooth walls. The tunnel has a contraction ratio of 17.8. The cavity plates were flush mounted with the bottom of the test section as seen in Figure 3. The design of the cavities will be discussed in the “DOE” subsection.

Measurements were taken over 24 wind tunnel runs. Twelve of these runs were with the acoustic source mounted and 12 were with only the plate mounted cavities. The entire speaker support was removed from the tunnel to minimize noise sources for the tunnel only runs. The cavity plates, presence of the acoustic source, and wind tunnel velocity were randomized between each run. Data were collected for all seven microphones simultaneously.

Acoustic source. A calibrated acoustic speaker, by Qsources BVBA, was used to produce an omnidirectional broadband noise source at a PWL of 45 dB. This is the maximum sustained output of the source. This source was chosen as it is designed for use in a wind tunnel and produces a constant sound intensity level between 0.3 and 7 kHz. The speaker produced a white noise signal. This was selected in order to replicate broadband airfoil trailing edge noise. A NACA 0018 profile support with a chord of 8 cm held the source 0.53 m above the cavities.

Data acquisition. Microphone measurements were made with a combination of LinearX M51 and M53 $\frac{1}{2}''$ condenser microphones. These microphones have a dynamic range of 122 (±1) dB up to 20 kHz. The microphone baffles were removed and the microphones were directly mounted at the base of each cavity. A National Instruments data acquisition system NI9215 acquired the pressure fluctuations measurements at 51,200 Hz. For every run, data for each cavity in the installed plate were captured simultaneously. Forty seconds of data were taken. Between each cavity configuration change, the microphone positions were redistributed randomly to reduce the likelihood of biased data due to microphone offset. The microphones were calibrated with a calibrated GRAS 42AA piston phone immediately after completing the measurement campaign.

Hot-wire measurements. A calibrated Dantec 1-channel hot-wire probe measured the velocity profile at nine different span-wise locations. The sample rate was 50 kHz with a 10 kHz low-pass filter with a 3% measurement uncertainty. Each span-wise measurement point corresponds to a cavity location. The probe was located 25 mm in front of each cavity. The boundary layer was measured at 30 and 70 m/s.

DOE

Cavity depth, diameter, mesh, chamfer, opening percentage, and boundary layer characteristics affect the spectral energy at the base of a cavity[4,9,10] and the SNR of the microphone measurements. These parameters were defined in terms of depth, diameter, mesh, chamfer, and opening percentage as discussed previously. These are the independent experimental variables that were varied during the experiment. This experiment was designed to quantify the relationship between these independent variables and the response variables (the spectral energy and SNR). Table 2 shows the variables, their type, and the maximum and minimum levels considered. These bound the potential design space and the resulting cavities are a combination of these geometric variables. To establish a model describing the relationship between these variables, each variable needs to be varied and the resulting response compared. One approach is to vary one variable or factor at a time while holding the others constant. This is known as the OFAT approach. For this experiment, OFAT would result in 1458 different potential combinations.[11] As this is not feasible, a subset of this design space needs to be selected for the test.

DOE[17] is a methodology used to optimize the selection of test variables, number of runs, and run order to support statistically sound analysis of the resulting measurements.

Table 2. Experimentally varied variables, type, and respective levels. All variables have an estimated power greater than 0.99.

Experimental variables	Type	Levels
Tunnel velocity (m/s)	Continuous	30, 70
Diameter (mm)	Continuous	5, 10
Mesh	Categorical	Yes, No
Depth (mm)	Continuous	0, 5, 10
Opening (%)	Continuous	50, 100
Chamfer (mm)	Continuous	0, 4

Specifically, it enforces randomization, statistical replication, and orthogonality in the experimental design. This is done by applying an optimization criterion to all the possible permutations of experimental variables to determine which subset of the experimental design space provides the most meaningful data. This resulting design allows for the development of an empirical model that evaluates the effect of experimental variables and the effect of their interactions on the response variables of interest. This methodology is widely used in many research fields as well as industrial applications[17,18] to design experiments that yield meaningful results while minimizing the number of experimental runs. For this experiment, DOE was used to select the combination of geometrical parameters that define each of the 12 cavities discussed previously and the run order. DOE enables an efficient use of test resources to characterize the effects different cavity geometries have on the TBL spectral energy and SNR with statistical confidence.

For this experiment, a D-optimal[17] design criterion was used to optimize the choice of the values of each experimental variable seen in Table 2, to fully evaluate their effect on the spectral energy and SNR. The selected combinations form the experimental design. This design is expressed as an $n \times m$ design matrix, $\boldsymbol{X}$, where m is the number of experimental variables and n is the number of experimental measurements, selected a priori.[17] Within the matrix, $\boldsymbol{X}$, each value of the experimental variable is normalized so that the lowest value is -1 and the largest value is 1. The D-optimal algorithm selects the combination of variables that maximizes the determinant of $\boldsymbol{X}^T\boldsymbol{X}$. This criterion also minimizes the correlation among experimental factors by maximizing the difference between the values of each variable for each run which is ideal for exploring a new design space.[17]

The results of this optimization are shown in Table 1. This DOE was performed using the *R* software package, *skpr*.[19] In addition to selecting the 12 cavities, the resulting experimental design also determined how many runs were required to measure sufficient data to develop a statistically sound empirical model. The resulting experimental design includes testing the cavities at two velocities, with and without an acoustic source, and with three replications which results in 144 total measurements. This compares favorably to the OFAT approach of 1458 different measurements, which would not include any statistically beneficial replications.

Experimental designs are evaluated by the resulting statistical power and the correlation between experimental variables. Statistical power is the probability that the experiment will result in statistically significant outcomes for each factor.[17] This design predicts that each experimental variable has a statistical power of greater than 0.95. Therefore, the significance level, α, is 0.05. Figure 4 presents the predicted correlation matrix between all of the

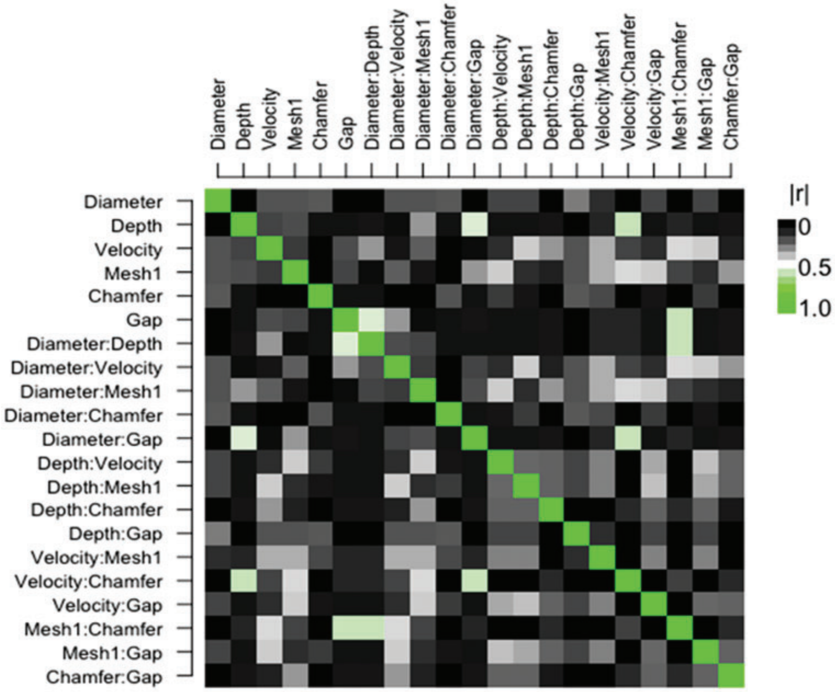

Figure 4. Correlation matrix of interaction between experimental variables.

variables. The correlation coefficient is calculated by dividing the covariance of the variables by the standard deviations of the same variables. This correlation defines the linear relationship between the two variables. The correlation between variables should be low, which suggests there is a sufficient number of runs to fully evaluate the design space without conflating the effect of two or more factors.[17] This is the case for all of the experimental variables; however, some of the interaction terms have higher correlations with some of the variables. This means that should these terms appear to be statistically significant during the analysis then it is important to study them closely before including them in the empirical model.

Experimental results

Boundary layer measurements

HWA measured the boundary layer properties at nine positions over the entire wind tunnel span and two free-stream velocities. The boundary layer profiles were measured 1.5 m downstream of the tunnel nozzle exit. Temperature variations in the free-stream flow are the primary source of measurement error due to the variation in tunnel temperature over the long time spent to characterize the boundary layer at each span-wise location. The recorded temperature range during each measurement campaign was used to correct the HWA measurements[20]

$$E_{w,r} = E_w \sqrt{\frac{T_w - T_r}{T_w - T_a}} \tag{4}$$

where $E_{w,r}$ is the temperature corrected hot-wire voltage, E_w is the measured hot-wire voltage, T_r is the hot-wire reference temperature, T_w is the hot-wire temperature, and T_a is the tunnel ambient temperature. The resulting profiles are shown in Figure 5(a). The boundary layer properties were calculated from the mean of HWA measurements. These properties are listed in Table 3. From the shape factor, H, it is evident that the boundary layer for both velocities is fully turbulent.

The measurements showed no variation in boundary layer properties with span-wise position. From these measurements the boundary layer thickness ($\delta 99$), momentum thickness (δ_θ), shape factor (H), friction velocity (u^*), and wall shear stress (τ_w) were calculated. Their mean values and 95% confidence intervals are shown in Table 3. The friction velocity was calculated[21] from τ_w. The shear stress was calculated from δ_θ using the Karman–Schoenherr relation.[22] These boundary layer properties were then used to normalize[21] the

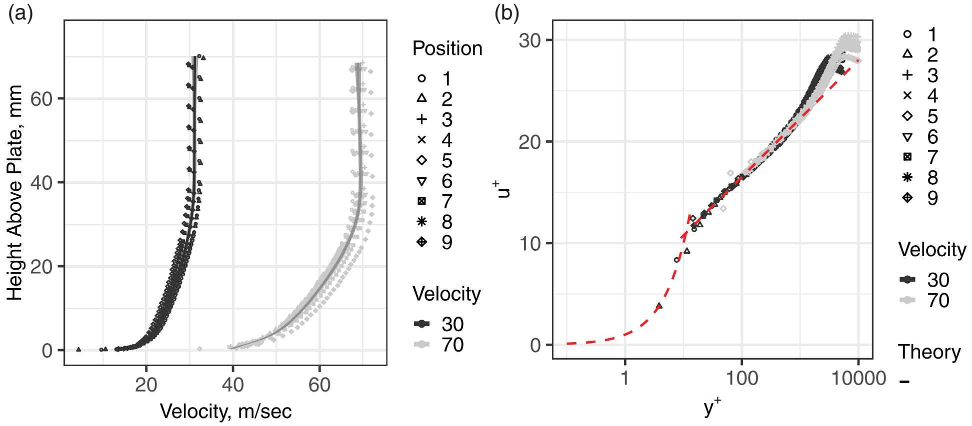

Figure 5. Boundary layer measurements. (a) Boundary layer velocity profiles measurements at span-wise positions and (b) boundary layer data logarithmic profile fit.

Table 3. Boundary layer properties, where Re_θ is the Reynolds number, δ_{99} is the boundary layer thickness, δ_θ is the boundary layer momentum thickness, H is the boundary layer shape factor, u^* is the friction velocity, and τ_w is the wall shear stress.

	Tunnel velocity (m/s)	
Properties	30.0	70.0
Re_θ	8627 ± 1330	$17{,}050 \pm 1103$
δ_{99} (mm)	50.7 ± 16.0	46.5 ± 9.47
δ_θ (mm)	4.35 ± 0.69	3.70 ± 0.24
H	1.33 ± 0.01	1.40 ± 0.04
u^* (m/s)	1.10 ± 0.02	2.40 ± 0.02
τ_w (Pa)	1.45 ± 0.04	6.96 ± 0.13

boundary layer profile in terms of $u^+ = \frac{u}{u^*}$ and $y^+ = \frac{yu^*}{\nu}$. For this fit it was assumed that the wind tunnel surface was smooth. The value of u^* is listed in Table 3. For the 30 m/s measurements, it was possible to get the HWA probe within 0.5 mm of the wall. For the 70 m/s case, it was only possible within 2.5 mm due to vibrations in the support sting.

Microphone measurements

The spectral energy level and SNR at the base of the cavities were evaluated between 250 Hz and 7 kHz, the frequencies typically of interest for aeroacoustic measurements of wind turbine blades. The analysis was performed for the 30 and 50 m/s runs due to some microphones being saturated for the 70 m/s measurements. These runs correspond with Reynolds numbers of 21,116 and 35,194 based on a 1 cm diameter cavity. Figures 6 and 7 illustrate the

Table 4. Twelve cavity geometries, Flush A and Flush B are the flush mounted microphones for each plate.

Designation	Depth (mm)	Mesh	Area (mm)	Change in area (×100%)
1A	5.0	Yes	254.5	−2.2
2A	10.0	Yes	78.5	0.0
3A	5.0	No	132.7	−5.8
4A	5.0	No	9.8	0.5
5A	10.0	Yes	127.2	−0.6
6A	5.0	No	78.5	0.0
7B	10.0	No	9.8	0.5
8B	10.0	Yes	19.6	0.0
9B	10.0	No	39.3	0.5
10B	10.0	Yes	132.7	−5.8
11B	5.0	Yes	127.2	−0.6
12B	5.0	No	66.4	−2.4
Flush A	0.1	No	28.5	0.0
Flush B	1.0	No	5.7	0.0

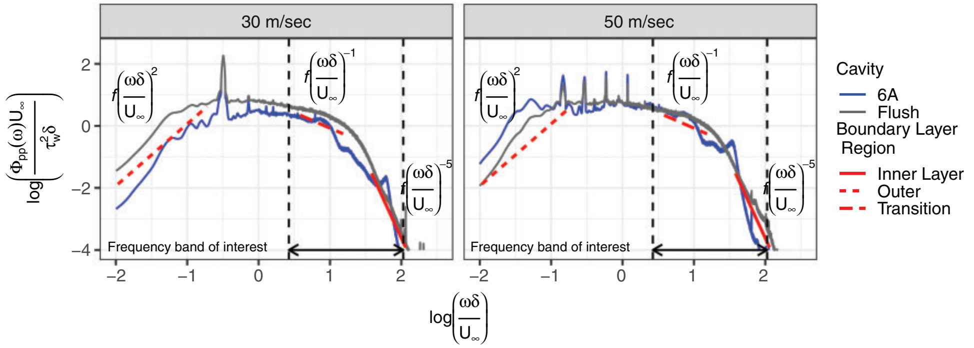

Figure 6. Cavity 6A, no mesh and no change in area, acoustic spectra normalized with the boundary layer properties. Vertical dashed lines demarcate the frequency band of interest.

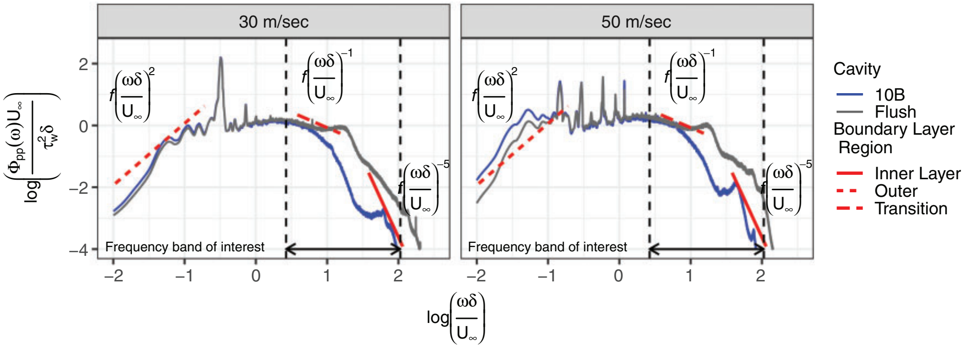

Figure 7. Cavity 10B, mesh with change in area, acoustic spectra normalized with the boundary layer properties. Vertical dashed lines demarcate the frequency band of interest.

influence of cavity design on the measured TBL spectral energy, Φ_{pp} compared to a flush mounted microphone. Spectral energy is normalized by free-stream velocity U_∞, wall shear stress τ_w, and the boundary layer thickness, δ_{99}. The angular frequency, ω is normalized by the ratio between δ_{99} and U_∞. The vertical dashed lines delineate the frequency region of interest. Cavity 6A is not covered with a stainless steel mesh and the cavity area does not change with depth. At the horizontal axis value of 1, the spectral energy is slightly less than the baseline flush case. Cavity 10B has a mesh and due to the added chamfer, the area decreases with depth. This cavity shows much less TBL spectral energy with respect to frequency as cavity 6A. This shows a clear effect due to covering the cavity with a mesh and having a change in the cavity area. The trend in spectral energy matches standard empirical trend lines in spectral energy for each region of the boundary layer.[5] Spectral energy is higher in the outer and transition region while it decreases toward the wall where the higher frequency fluctuations are generated. For all of the cavities, reductions in the energy spectra were generally seen at frequencies above 1.5 kHz or normalized at values of 0.75 in Figures 6 and 7. Comparing the spectral energy at the base of each cavity provides insight into the effect of cavity geometry; fitting an empirical model allows for the effect of cavity geometric parameters to be evaluated separately. This allows us to quantify and interpret why one cavity is more effective at attenuating TBL noise than another.

Establishing an empirical model

Two empirical models were developed to describe the relationship between the response variables, spectral energy and SNR, and the cavity geometric parameters for different tunnel velocities. These were calculated from the power spectral density of the microphone data. The inputs to the model include cavity depth, area of the cavity opening, and change in area with depth if there is a chamfer or partial covering over the cavity, and whether or not a mesh covered the cavity. Additional terms include the wind tunnel free-stream velocity and which microphone was used for measurements. Since both response variables are frequency dependent, frequency was included as a model term. Initially a generalized linear mixed model (GLMM) was fit to the data. This provided insight into the relationship between the model terms and the response variables but due to the non-linear dependence on frequency, a GAM was implemented.

Data preparation

The response variables, spectral energy and SNR, were calculated over the frequency range of interest (250–7500 Hz). Figures 6 and 7 show the relationship between frequency and the spectral energy response variable and thus the importance of including this dependency in the analysis. A bandwidth of 50 Hz was selected in order to accurately capture the relationship between the response variables and frequency while maintaining a reasonable computational time.

Initial linear modeling

Generalized linear mixed effect models are widely used for interpreting experimental results. The advantage of this model over standard linear regression is that both fixed and random effects can be included in the model.[23] Equation (5) represents a generalized linear mixed effects model

$$\boldsymbol{y} = \boldsymbol{X\beta} + \boldsymbol{Zb} + \epsilon \tag{5}$$

Here $\boldsymbol{y}$ is an n-vector of the response variable (spectral energy or SNR) at each cavity geometry, frequency band, and velocity. The vector length n is then the number of experimental observations which is $n_{cavity} \cdot n_{bands} \cdot n_{velocity} \cdot n_{replications}$. For this experiment there were 11,508 observations. $\boldsymbol{X}$ is an $n \times m$ design matrix where m is the number of model terms. Each column contains the continuous variable values such as the geometric parameters (cavity area, depth, and change in area with depth), frequency, and tunnel velocity. The microphone used for the measurement as well as the presence of a mesh are modeled as categorical variables which result in a column for each variable with a value of either 1 or 0 within the respective column. Additionally, the interactions between these terms are included as additional columns. $\boldsymbol{\beta}$ is an m-vector containing the unknown coefficients of the linear model corresponding to the columns of the design matrix. $\boldsymbol{Z}$ is the design matrix of random observations or known sources of error. It has dimensions $n \times p$, where p is the number of random variables, whose values are fixed at the p-vector $\boldsymbol{b}$. ϵ is the model error or residuals, an n-vector.

A mixed effects model was chosen because it allows for known sources of error to be accounted for as random effects. For this experiment, tunnel velocity and the microphones are specified as random effects. Velocity is accounted for as a random effect to separate it from $\boldsymbol{X}$. This approach improves the estimate of the effect size of each geometric parameter because all of data points are used to create one estimate with the differences due to velocity being accounted for a separate variable. This is in contrast to grouping the data into separate groups for each velocity and calculating the effect size within each group. By using more data points, the fit of the model is improved. Modeling the microphones as random effects enabled any bias in the measurements due to a specific microphone to be accounted for separately from the geometric parameters of interest.

The results obtained from the linear mixed model showed that parameters such as depth, mesh, and change in area were significant and that their effect is congruent with previous experimental data and physical intuition. For example, an 8 dB reduction in spectral energy can be attributed to the presence of the mesh. However, this linear model does not capture the non-linear dependence of the spectral energy with frequency. This is shown by plotting the residuals of the model in Figure 8(a), which shows the heteroskedasticity of the linear

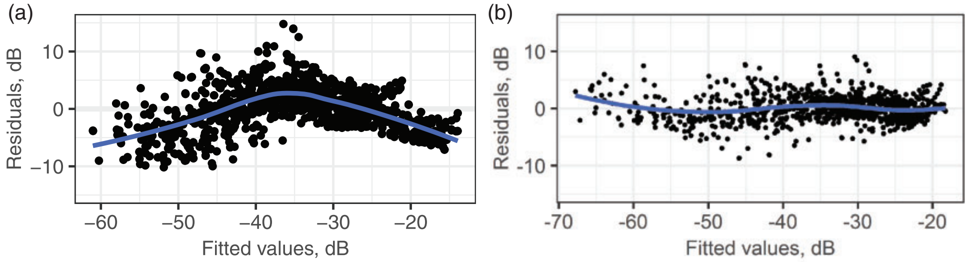

Figure 8. Comparison of the effect of model selection on residual distribution. (a) The residual distribution for the linear model shows heteroskedasticity and (b) the residual distribution for the GAM shows improved homoscedasticity.

model residuals as described by equation (5). Heteroskedasticity is when the variance of residuals is not randomly distributed about 0. This suggests that a linear model may not be suitable to fully evaluate how the effect of different experimental factors changes with frequency. For this reason, an extended model that allows for using splines to model non-linear terms was investigated.

GAM

Following the GLMM model development, a GAM was developed to model the data set. GAMs can be thought of as extensions of linear models. The primary difference is that instead of only linear terms, GAMs allow for the experimental factors x_i, from the matrix $\boldsymbol{X}$, to be modeled with smooth splines.[24] Notionally, the coefficients in a linear model are replaced by smooth splines as shown in equation (6), where $f(x_{im})$ are splines that replace the coefficients in $\boldsymbol{\beta}$, and β_0 is the model intercept. The ith entry of y is then represented as equation (6)

$$y_i = \beta_0 + f_1(x_{i1}) + f_2(x_{i2}) + \ldots + f_m(x_{im}) + \epsilon_i \quad i = 1 \ldots n \tag{6}$$

Each spline term is the estimate of the contribution of each experimental factor to the overall response variable. These terms are additive and when combined result in the estimate of the response variable. These splines can represent individual factors or combinations of factors, known as interaction terms. GAMs can also be applied to mixed effect modeling as discussed previously. Figure 8(b) shows the improvement over a linear model. The curve of the mean residual distribution is now much closer to the ideal zero mean line which is known as homoscedasticity. Additionally, the magnitude of residuals is also smaller, implying a better fit of the data. GAMs were fit to both the SNR and the spectral energy response variables data sets using the *lme4 R* package.[23] When goodness of fit is compared between the GAM and the GLMM, the GAM is a better model. Goodness of fit can be evaluated in terms of the Akaike information criterion (AIC), the percent of deviance explained by the model, and the residuals. AIC is a standard metric which combines an expression for the goodness of fit with the number of parameters used to fit the model.[17] A lower AIC is better but this can only be used to compare models based on the same data set, which is the case here. The AIC for the GLMM is 63,350 and for the GAM it is 58,162.

TBL spectra

A GAM was developed to examine the relationship between the wall pressure spectral energy and the experimental factors. Given that the spectral energy response variable decays with frequency[14] with a non-linear dependence, as shown in Figure 7, it is important to model the spectral energy as a non-linear function of frequency. Applying a GAM allowed this term to be modeled with a spline, which resulted in a substantial model improvement compared to the GLMM.

Fitting the spectral energy GAM to the experimental data requires careful consideration of potential model parameters. Parameter selection is a balancing act between explaining as much variance in the data as possible while avoiding over fitting the model by including all possible model terms. Model parameters were added and removed progressively, beginning with a random effects only model that contained tunnel velocity and the microphones. As model parameters were included and removed, subsequent model iterations were compared against this random effects only model. In generalized additive modeling, parameters can be added as linear parameters or as spline basis functions (applied to the response variables with a frequency dependence) which estimate the non-linear relationship between the response variable and the experimental parameters.

Each geometric parameter was added as a model parameter. After each one was incorporated, the updated model was compared against the initial random effects only model. The AIC was used as selection criterion during this process. In parallel to using the AIC to optimize the model, the distribution of residuals was also considered. Ideally, residuals should be normally distributed and as close to zero as possible.[24] The size of the residuals and their shape when plotted is a tool for indicating whether the model is missing a key parameter. Large residuals suggest that the model is missing a term that explains the source of variance. The heteroskedasticity of the residuals also implies that there is a non-linearity that the model does not account for. Finally, the physical interpretation of model parameters was an important consideration. In practice this means that instead of fitting all model terms and removing those that have p-values > 0.05, the model terms need to have a physical explanation. For example, both the cavity depth and presence of a mesh covering have physical interpretations. It is assumed that a mesh can be modeled by imposing an impedance across a cavity opening. As discussed previously, equation (1) suggests that cavity depth can be explained by cut-off modes decaying exponentially with distance.[12] This exponential relationship for depth was linearized by taking the natural log in order to better model the relationship between depth and spectral energy. In contrast, if a model parameter had a small coefficient and did not have a physical significance, it was removed even if it was statistically significant. Once evaluating the inclusion of cavity depth, change in area, area, and mesh, including the interactions between these terms was evaluated using the same approach. Being able to evaluate interactions is an important benefit of using DOE methods.[11,18] This model selection approach avoids over fitting the model to the data. The risk of an over-fitted model is that by tuning a model to explain as much of the variance in the data as possible, it is possible to get a model that is less accurate when applied to other data sets. By avoiding over fitting, this GAM supports future comparison to analytical models, computational fluid dynamics (CFD) simulations, and experiments.

Table 5 compares the random effects only GAM with the final GAM as well as the GLMM. The final GAM has a reduced AIC and dispersion. The R^2 value increased from 73 to 92% compared to the random effects only model. Figure 9 shows the residual

Table 5. Cavity spectral energy statistical models comparison.

	Linear mixed model	Random effects only	Final model
AIC	63,350.39	74,592.22	58,162.02
Log likelihood	−31,665.19	−37,277.37	−29,038.42
Num. obs.	11,508	11,508	11,508
Dispersion (variance)	13.3	38.17	9.14
R^2	0.90	0.73	0.93
Num. smooth terms	0	3	7

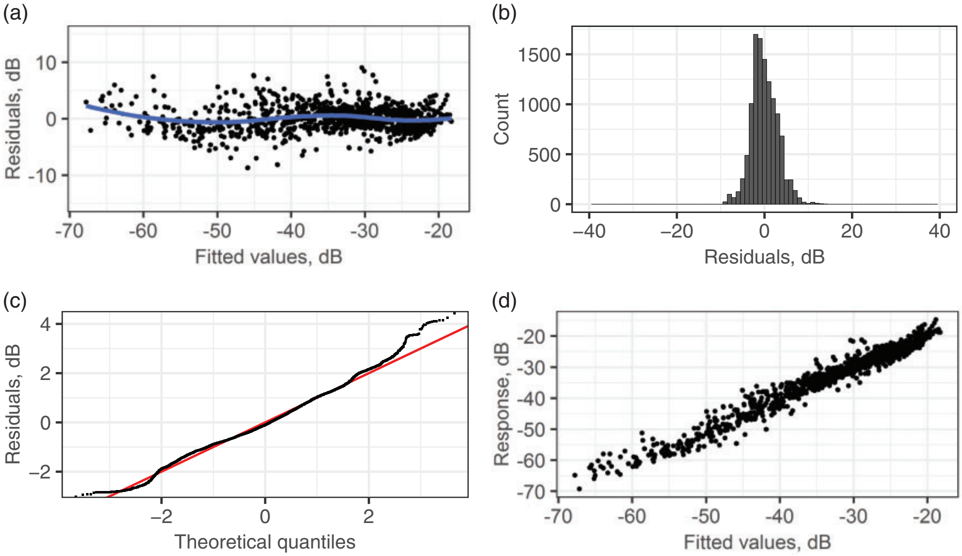

Figure 9. Boundary layer spectral energy GAM model residual diagnostic plots: (a) Homoscedasticity of residuals, (b) histogram of residuals, (c) quantile-quantile plot, and (d) model response versus measured values.

diagnostic plots using the final GAM. The histogram in Figure 9(b) shows that the residuals are close to zero and indicates that they are normally distributed. This is further supported by the quantile-quantile plot, Figure 9(c), which plots the probability distribution of the model residuals against a normal distribution. Since the residuals are close to the line, this supports the assumption that the residuals are normally distributed.[24] Figure 9(a) shows that the model residuals are homoscedastic as they are closely distributed around zero, indicating that there are no non-linear effects remaining unincorporated into the model. Figure 9(d) compares the experimental data with the model prediction. As shown, these points are closely distributed around a slope of one, indicating that the model adequately represents the data.

The estimated individual contributions to the spectral energy for each of the model parameters are listed in Table 6. Depth, area, change in area, and presence of mesh are shown to be statistically significant (p-values < 0.05) linear model parameters. Two significant interaction model parameters are the interactions between the presence of a mesh and

Table 6. Cavity spectral energy model parameters.

Linear parameters	Coefficients, dB (standard error)
(Intercept)	−61.48 (0.325)***
Area	−0.02 (0.002)***
log (Depth)	−0.64 (0.029)***
Change in area	1.67 (0.042)***
Mesh Yes	−6.56 (0.153)***
Change in Area × Mesh Yes	−1.56 (0.053)***
Area × Mesh Yes	−0.02 (0.002)***
Spline parameters	**Est. degrees of freedom (standard error)**
s (Frequency)	6.99 (7.94)***
s (Microphone)	7.89 (8.00)***
s (Tunnel velocity)	1.00 (1.00)***
s (Frequency) × Mesh Yes	7.90 (8.59)***
s (Frequency) × Resonance Yes	8.69 (8.95)***

***$p<0.001$, **$p<0.01$, *$p<0.05$.

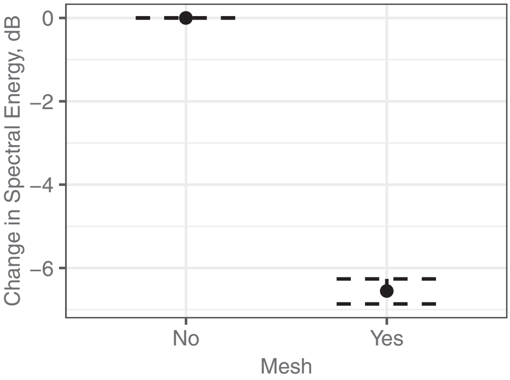

Figure 10. Effect size of mesh linear term.

that of the cavity area and change in area. Parameter coefficients are also commonly referred to as the parameter effect size for the linear coefficients. These values are interpreted by multiplying this coefficient by the value of the model term. For example, for a cavity that has a depth of 10 mm, the overall change due to depth is $\ln(10) \cdot (-0.64) = -1.5$ dB. It is important to note that despite the area term having a small coefficient, its net contribution to the model is still substantial. This is because the area is on the order of 100 mm^2 and when multiplied by −0.02 results in a reduction around 2 dB. The mesh is estimated to reduce the spectral energy by 6.5 dB, Figure 10, which is in agreement with previous experimental work.[9,10] The interaction terms are interpreted by multiplying all terms in the interaction by the coefficient, e.g. the value of the area multiplied by the coded value for the mesh, 1, by −0.02. This shows that there is a greater reduction in the spectral energy with increasing area if there is a mesh present. For the other interaction term, the change in area only reduces the spectral energy when there is no mesh. Otherwise, changing the area has minimal effect. To predict the amount of spectral energy for a given geometry, these linear terms, the model intercept, and the spline terms are summed together.

Spline basis functions for frequency, mesh with frequency, and resonance with frequency were included in the GAM. Given that spatial averaging of turbulent structures is dependent on the transducer area as described by Corcos,[25] a spline term for the variation in spectral energy due to area with respect to frequency was considered. However, the predicted reduction in spectral energy for the frequencies and cavity areas considered was relatively small at approximately 2 dB and the resulting spline term showed an even smaller reduction in spectral energy with frequency due to cavity area. Therefore, this term was neglected in favor of simplifying the model. The resonance term was added to account for a peak in spectral energy around 5000 Hz present for some cavities due to a piston mode, in order to avoid attributing this peak to other model terms. As with the previously discussed spectral energy model, tunnel velocity and the microphone were modeled as random effects. Table 6 lists the final model parameters and their estimated degrees of freedom. The estimated degrees of freedom should be lower than the number of degrees of freedom for each variable which is important to avoid over fitting the spline. This table shows that the following splines are statistically significant: spectral energy with respect to frequency, spectral

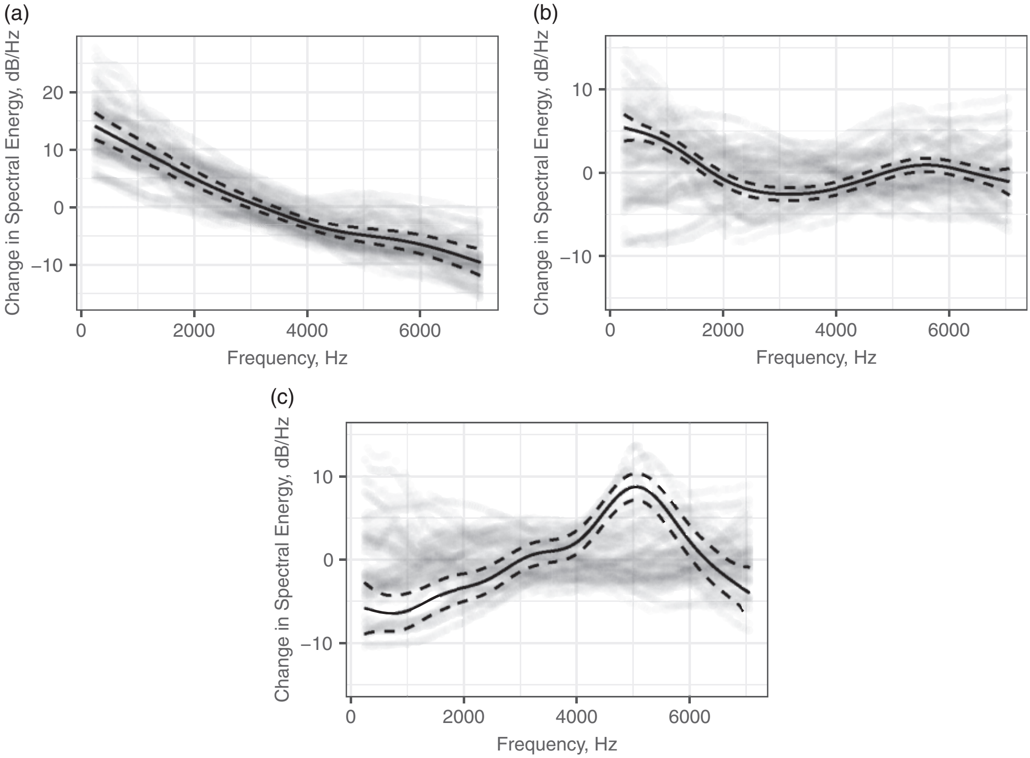

Figure 11. Change in spectral energy with frequency GAM splines. The dashed lines are 95% confidence intervals. Gray points are the observed data. (a) Estimated change in spectral energy with frequency, (b) estimated change in spectral energy due to mesh with respect to frequency, and (c) estimated change in spectral energy due to resonant modes with respect to frequency.

energy and the mesh with respect to frequency, and the presence of a resonant mode with respect to frequency. Unlike the linear terms, the spline terms cannot be interpreted solely from a table of coefficients. They need to be analyzed graphically. Figure 11 shows these three splines. Figure 11(a) shows the decay in spectral energy with increasing frequency. Figure 11(b) shows how the influence of mesh is frequency dependent. When this plot is combined with the linear component of the mesh as shown in Figure 10, −6.5 dB, a net reduction of 10 dB is estimated at 3000 Hz. Given that for most materials impedance often is frequency dependent, this dependence is expected. However, additional experiments are required to determine how geometry of the mesh (e.g. thread diameter and density) influences this relationship. Finally, Figure 11(c) shows the resonant mode peaking at 5000 Hz. When these spline terms are combined with the linear terms in Table 6 the combination estimates the total spectral energy for an arbitrary cavity geometry.

By using a mixed effects model, the presence of microphone bias was confirmed. Figure 12 shows that several microphones have a measurement offset that is statistically significant compared to the other microphones. The microphones should be statistically indistinguishable from each other and centered around 0 dB; however as an example, microphone 7 is shown to have the largest offset, with a 2.5 dB bias compared to the other microphones. By accounting for this in a mixed model, the measurement error in the response variables due to the microphones is accounted for and does not influence the results by biasing the data toward measurements made with a specific microphone. This bias was only detectable due to randomizing runs and randomizing which microphones were used with which cavity among runs.

SNR

Using cavities to reduce the boundary layer energy at the microphone is only useful for aeroacoustic testing if the acoustic signal of interest is not reduced proportionally with the reduction in TBL noise. The ratio between the signal of interest and background noise due to the boundary layer is the SNR. For this experiment, the runs to measure the pressure fluctuations of the boundary layer were repeated with an acoustic source in the center line of the wind tunnel. The intent of this set-up was to be able to compare the spectral energy of the source with that of the boundary layer. However, for most cavities, the acoustic

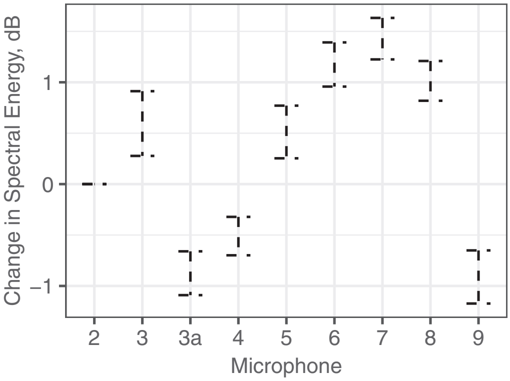

Figure 12. Effect of microphone measurement bias with 95% confidence intervals.

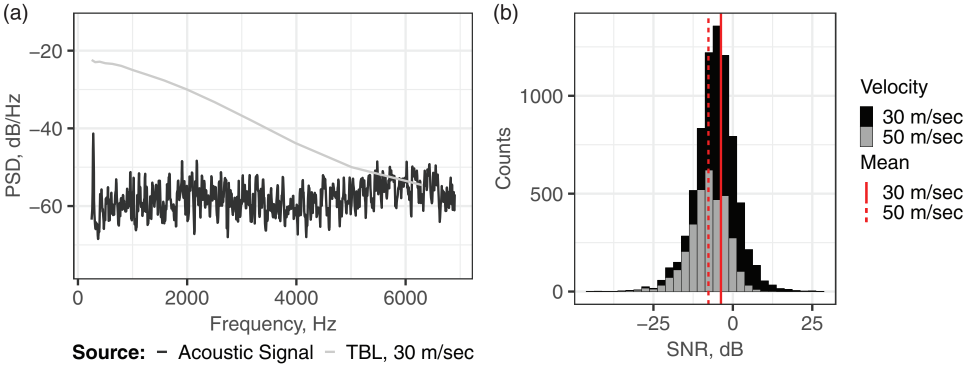

Figure 13. Signal power spectral density (PSD) level compared to boundary layer pressure power spectral density levels. (a) Spectral energy comparison for flush mounted microphone and (b) effect of velocity on SNR. PSD: Power spectral density.

energy was lower than the boundary layer energy, at frequencies below 6 kHz as shown in Figure 13(a). This figure compares the spectral energy of the boundary layer measured by a flush mounted microphone with the acoustic source without flow. The omnidirection source had a maximum PWL of 45 dB which was not sufficient to adequately characterize the SNR. Both the boundary layer pressure fluctuations and the acoustic source are broadband sources. Extracting the signal level from the noise level is non-trivial. The SNR was estimated using equation (7) where $P_{signal+noise}$ is the spectral energy with the acoustic source and $\bar{P}_{noise}$ is the average spectral energy per cavity with no source with respect to tunnel velocity and frequency

$$SNR = 10\log_{10}\left(\frac{P_{signal+noise} - \bar{P}_{noise}}{\bar{P}_{noise}}\right) \tag{7}$$

The average boundary layer spectral energy, $\bar{P}_{noise}$, for each cavity was calculated with respect to frequency and velocity resulting in an average spectrum for each cavity at both 30 and 50 m/s. The resulting average ensemble was subtracted[4] from each run with the acoustic source at matching velocities. This was done over the frequency range of 250 Hz to 7 kHz. The resulting distribution of the SNR shows that most are below 0 dB as shown in Figure 13(b). This process introduces uncertainty because variation in the signal level between runs was approximately ±2 dB. If the difference between $\bar{P}_{noise}$ and $P_{noise+signal}$ is within this variation, it is difficult to determine if the signal is above the noise level. Given that 70% of SNR values are within ±2 dB, this is a significant source of error.

A GAM was developed to fit the SNR response variable to the experimental parameters. The objective was to identify the influence of the cavity geometry on SNR. Due to the errors introduced by calculating SNR for the comparatively weak acoustic source, the resulting statistical model does not fully explain the sources of variance. As with the spectral energy model, an initial random effects only model was developed as a starting point. Velocity and microphones were modeled as random terms. SNR decreases with increasing velocity, as shown by Figure 13(b). An iterative process of adding and removing model parameters was

Table 7. Cavity SNR statistical model diagnostics.

	Random effects only	Final model
AIC	48,724.67	46,147.91
Log likelihood	−24,351.47	−23,043.40
Dispersion	37.41	26.51
R^2	0.14	0.39
Num. obs.	7541	7541
Num. smooth terms	2	5

AIC: Akaike information criterion; SNR: signal-to-noise ratio.

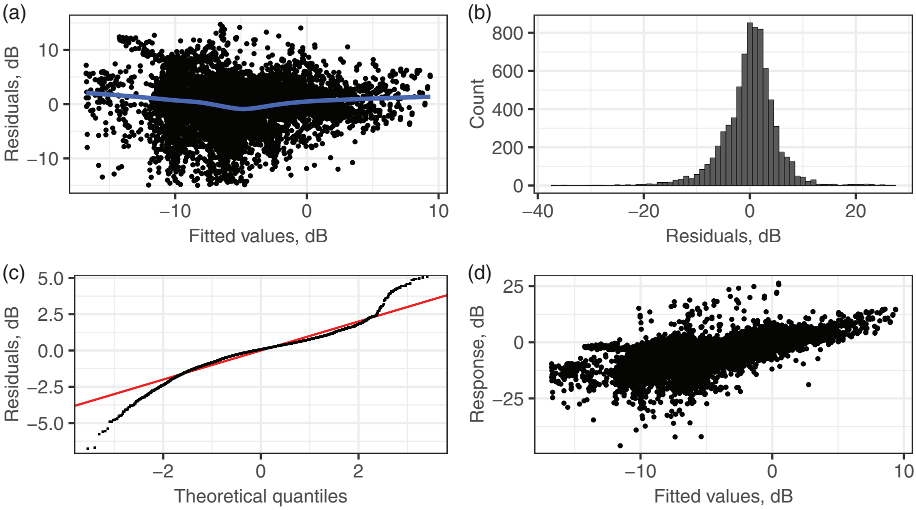

Figure 14. SNR GAM model residual diagnostic plots: (a) Homoscedasticity of residuals, (b) histogram of residuals, (c) quantile-quantile plot, and (d) model response versus measured values.

followed using the same criterion as performed in the development of the spectral energy model. Frequency was the initial parameter included as a spline due to SNR increasing non-linearly with frequency, as inferred from Figure 13(a) which shows the energy level of the acoustic source and boundary layer converging with increasing frequency. This increase is due to the decay in boundary layer energy with frequency. The linear and non-linear terms for the geometric factors and their interactions were iteratively added and removed as before. The resulting model shows that the mesh, depth, change in area, as well as the interaction terms—depth and change in area and mesh and change in area—are statistically significant terms. This is consistent with the GAM developed for TBL spectral energy.

The final model explains more of the SNR variance in the data than the random effects only model as detailed in Table 7. The AIC and dispersion are lower, and the percentage of variance as expressed by R^2 is higher. These three diagnostic terms show that the final model is a better fit of the data. The final SNR model is only marginally better at explaining the variance in the data as quantified by the R^2. This is due to the uncertainty in the data stemming from the SNR calculation; this model only explains 39% of the variance.

Table 8. Cavity SNR model parameters, standard error is listed parenthetically.

Linear parameters	Coefficients, dB (standard error)
(Intercept)	0.37 (0.47)
Mesh Yes	1.96 (0.22)***
log (Depth)	−0.27 (0.07)***
Change in area	−3.87 (0.29)***
Mesh Yes×Change in area	−1.67 (0.14)***
log (Depth)×Change in area	2.24 (0.18)***
Spline parameters	**Est. degrees of freedom (standard error)**
s (Frequency)	4.93 (5.99)***
s (Microphone)	7.60 (8.00)***
s (Frequency)×Mesh Yes	7.27 (7.80)***
s (Tunnel Velocity)	1.00 (100)***

SNR: signal-to-noise ratio.
***$p<0.001$, **$p<0.01$, *$p<0.05$.

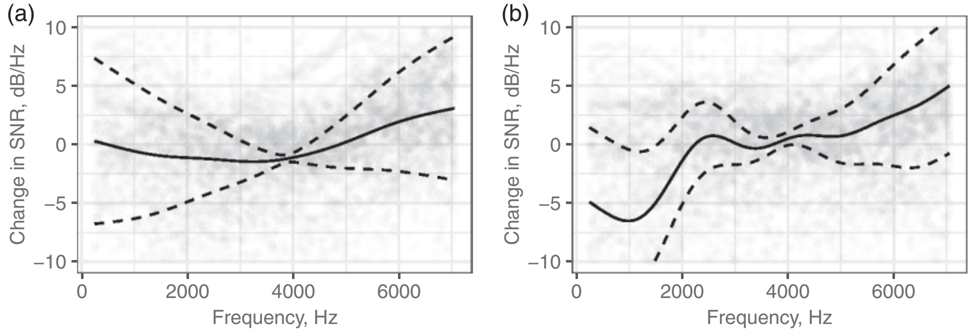

Figure 15. SNR GAM spline models. (a) Change in SNR with frequency and (b) change in SNR due to the mesh with frequency. SNR: signal-to-noise ratio.

The final model was also compared against the random effects model with a χ^2 statistical test and is significant with a $p \ll 0.001$. The resulting diagnostic plots for the final model in Figure 14 show that assuming the residuals to be normally distributed is reasonable. Figure 14(a) shows that the sources of non-linearity have been reduced due to the GAM. However, the dispersion of the residuals is large compared to that of the spectral energy, 26.5 dB (Table 7) and 9.1 dB (Table 5), respectively. The source of this dispersion is attributed to the uncertainty introduced through the calculation of SNR.

Table 8 lists the linear and non-linear terms for the SNR model. All of the terms in the model are significant with p-values $\ll 0.001$. The mesh improves the overall SNR by 2 dB and has a non-linear dependence on frequency, as shown in Figure 16. When the linear and non-linear terms are combined (Figures 15(b) and 16), the mesh increases the SNR by 5 dB at 6 kHz. The influence of the mesh is intuitively given since it reduces the energy of the boundary layer hydrodynamic fluctuations impinging on the microphone. The positive value for the depth linear coefficient suggests that SNR decreases with increasing depth.

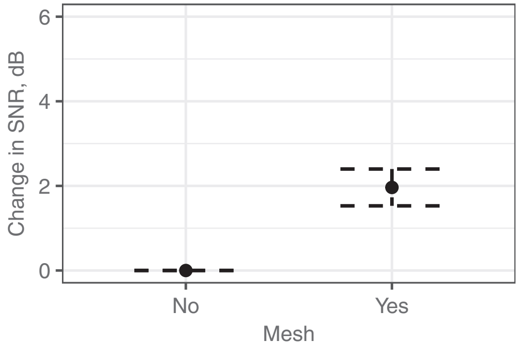

Figure 16. Change in SNR due to mesh. SNR: signal-to-noise ratio.

As the microphone is moved further from the acoustic source, the acoustic energy received at the microphone is lower. Because the acoustic waves from the speaker are assumed to be plane waves, the energy decays with the inverse square of the distance due to geometrical spreading. This suggests cavity depth should not have a substantial effect on the acoustic signal because the depths of the cavities are at most 1 cm compared to the 0.75 m distance between the speaker and the cavity. Plane waves do not decay at the same rate as the boundary layer pressure waves because the plane waves are cut-on while the other waves have modes that are cut-off within the cavity. Therefore, it is suspected that the increasing depth reduces the SNR. Further study is required to determine if this measured effect is real or due to the uncertainty in the SNR estimation. Changing the cavity area has a significant effect on increasing the SNR which is logical given that this parameter reduces the boundary layer spectral energy. The interactions terms involve the change in depth and the presence of the mesh interacting with the change in area. The mesh combined with the change in area increases the SNR. However, the increase due to the change in area is not substantial without the mesh present. The final interaction term between depth and the change in the area suggests that there is a minimal change in SNR with depth if there is no change in area. This suggests that changing the cavity area is more important to improving the SNR than the depth term. Given the uncertainty present in the data set due to the calculated SNR, it is difficult to state unequivocally which geometrical parameters have an important effect on the SNR. Future experiments should incorporate an acoustic source with higher power levels to achieve an SNR that is significantly higher than those seen in this experiment. This would reduce the uncertainty and result in a better GAM for SNR.

Model predictions

The spectral energy and SNR model predictions are useful in the evaluation of how the cavity geometric parameters affect the response variables of interest. The predicted values were calculated by using the cavity geometries as previously discussed in Table 4 as the input to the model. The resulting data were used to evaluate the net effect different combinations of cavity geometries have on spectral energy and SNR.

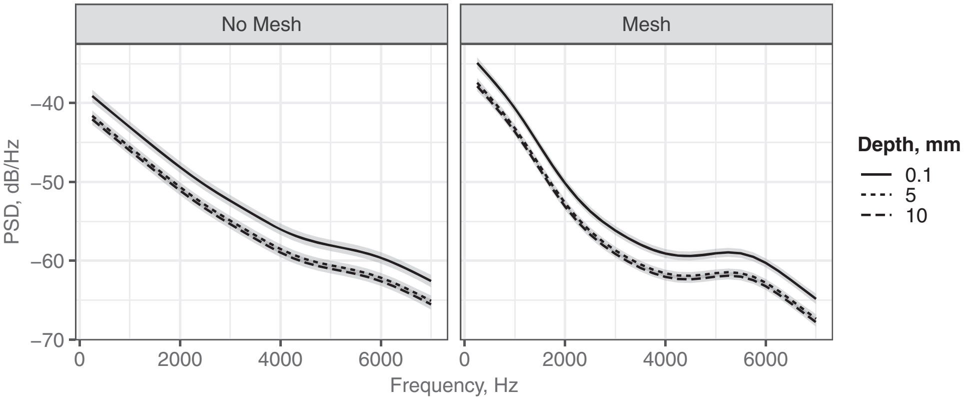

Figure 17. Effect of increasing depth on boundary layer power spectral density. PSD: Power spectral density.

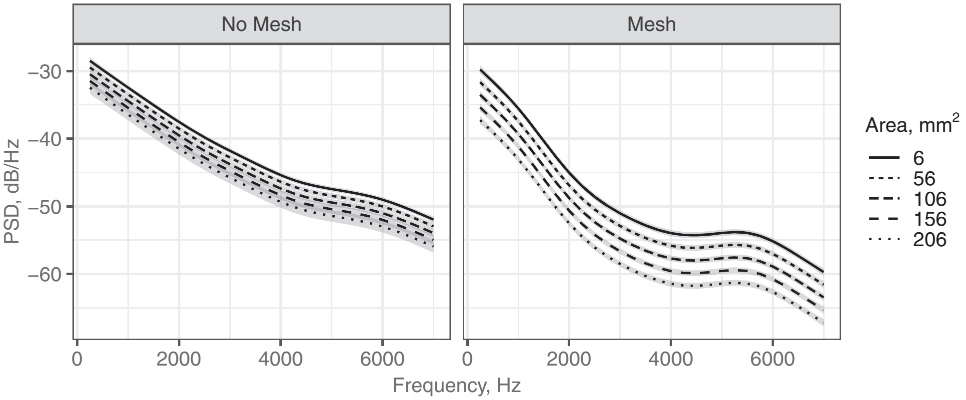

Figure 18. Effect of interaction between cavity opening area and mesh on boundary layer power spectral density. PSD: Power spectral density.

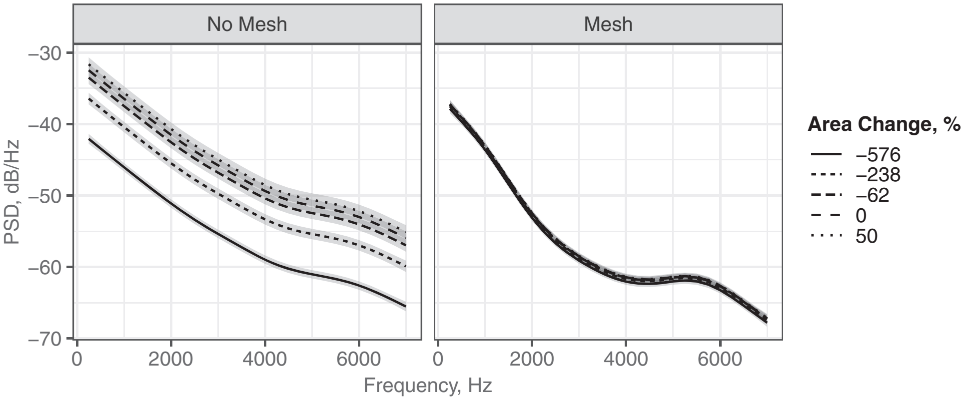

Figure 19. Effect of changing cavity area with mesh on boundary layer power spectral density. PSD: Power spectral density.

Spectral energy predictions

The GAM spectral energy predictions provide a basis for interpreting how the cavity depth, area, change in area, and presence of a mesh influence the spectral energy. Figures 17 to 19 depict the total change in spectral energy as a function of different parameters. Figure 17 shows the reduction in spectral energy with depth. Increasing depth has an exponential relationship with the overall reduction in spectral energy as described in equation (1). It is predicted that the deeper the cavity is, the less effective depth is at reducing the spectral energy. This is logical as the cut-off modes decay rapidly with distance and at a certain depth only the cut-on modes will continue to propagate. This figure also depicts the mesh reducing the spectral energy. The attenuation due to the mesh is frequency dependent and can be modeled as an impedance as described by equation (3). There is no interaction between the mesh and depth factors as shown by the fact that the change in energy with depth is constant between the two plots. Figure 18 shows that increasing the cavity area reduces the spectral energy measured by the microphone. This figure also shows the interaction between the mesh and the area term in the model. When a mesh is present, the cavities with a larger area show a much larger reduction in spectral energy. The underlying physical explanation for this interaction necessitates further investigation but a possible explanation is that the mesh reduces the energy in the hydrodynamic modes resulting in weaker cut-on modes for larger diameters. Reducing the area of the cavity from the aperture to the base of the cavity reduces the spectral energy as shown in Figure 19. However, the reduction due to this area change is only significant when there is no mesh. It is known from duct acoustics that changing the cross sectional area causes reflections that reduce the transmitted wave energy.[12] A possible explanation is that the mesh reduces the energy in the transmitted pressure waves to the point that when the area is reduced, the effect on the transmitted energy is insignificant.

SNR predictions

The SNR GAM predictions aggregate the model parameters into a predicted value for the SNR. This model output delineates how the cavity geometric parameters and their interactions influence the SNR. Figure 20 depicts how shallower cavities have improved SNR

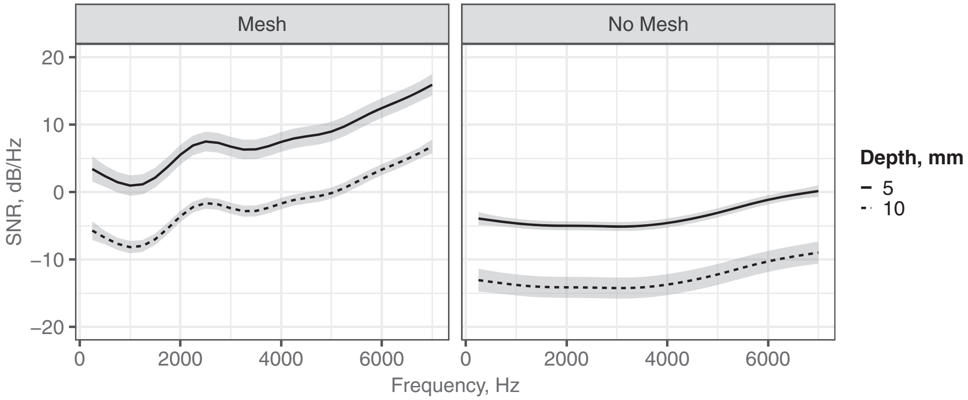

Figure 20. Change in SNR with increasing depth. SNR: signal-to-noise ratio.

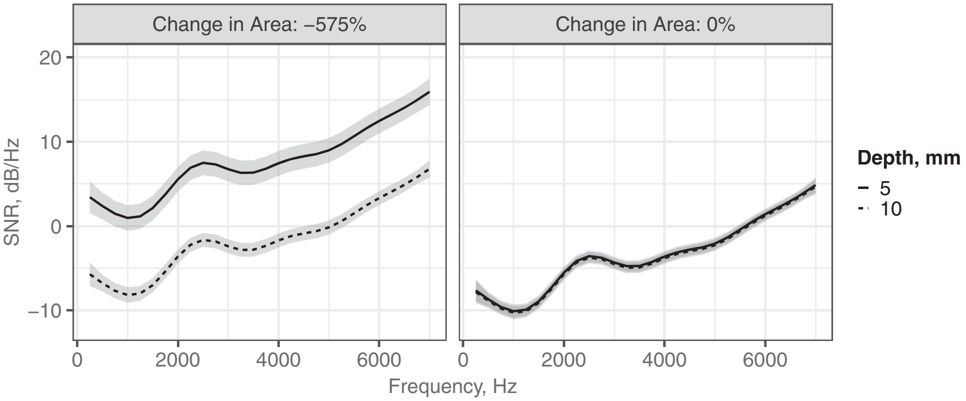

Figure 21. Change in SNR due to the interaction between change in area with depth. SNR: signal-to-noise ratio.

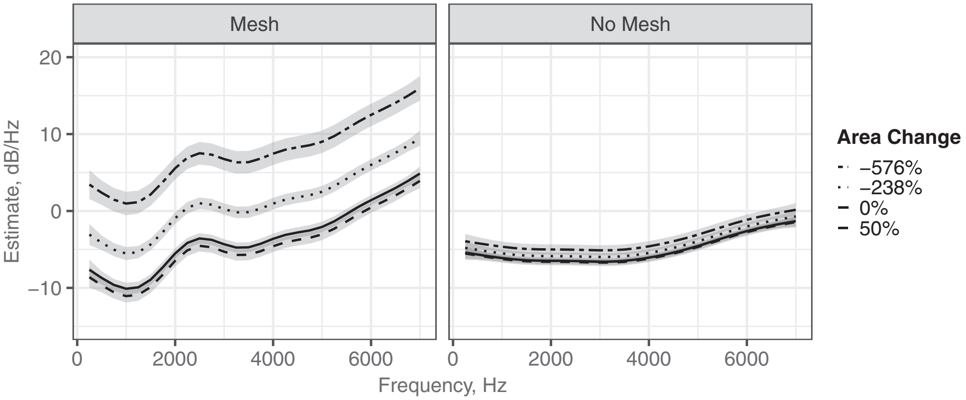

Figure 22. Change in SNR due to change in area with and without a mesh.

performance. However, there is no interaction between cavity depth and the presence of a mesh. Therefore, the mesh increases the SNR independently of the depth. The model predictions show a 7 dB improvement in SNR with decreasing depth. This raises questions because the TBL GAM shows a significant reduction in spectral energy, which should correspond to an increase or minimal change to the SNR. Unlike the spectral energy model, there is an interaction between the change in area and the cavity depth. Figure 21 shows that when the area of the cavity is reduced by 575% with respect to the aperture of the cavity, a shallower cavity has a higher SNR. Cavities with a constant area show an insignificant change in SNR with increasing depth. SNR increases with reduction in the cavity area. This is shown in Figure 22. This implies that the hydrodynamic fluctuation component of the signal is more affected by the changing area than the acoustic component. This improvement is amplified by the presence of the mesh. For that case, a 10 dB improvement in SNR can be seen when reducing the cavity area by 575% compared to the cavity with no change in area. This is logical as the pressure spectra at the microphone decrease with decreasing area as seen in Figure 19.

Conclusion

This study used DOE to systematically evaluate the effect of cavity geometry on pressure spectral measurements when a microphone is mounted on the base of a cavity. The DOE approach supported the development of empirical models that quantify the effect individual geometric factors including depth, area, mesh, and change in area have on the reduction in TBL spectral energy and increasing the SNR of an acoustic source. This approach provides a statistically rigorous framework for the experiment plan and follows on analysis while making efficient use of test resources.

A GAM quantified the effect of individual cavity geometric parameters and some of their mutual interactions have with respect to the two response variables. GAMs provide insight into the non-linear relationship between cavity geometries and the response variables over the frequency range of interest. This modeling approach is well suited for the boundary layer spectra and shows that the mesh reduces the spectral energy by 10 dB when the linear and non-linear terms are combined. It also shows that energy decreases exponentially with increasing depth. Finally, it quantified the relationship between the amount of reduction in cavity area and the presence of a mesh. The GAM fit of the SNR data was complicated by the fact that error was introduced by estimating the response variable by subtracting the empty tunnel spectra. Despite this, the model shows that a mesh improves the SNR by up to 5 dB and that having a cavity area that reduces with depth increases the SNR as well. Theoretical solutions to the wave equation for the propagation of pressure waves within a cylinder provide a framework for understanding how the hydrodynamic and acoustic waves propagate within the cavity. These inferences agreed with the statistical model.

The experimental results and the explanatory stochastic model are initial steps in developing a framework for designing microphone cavities to enable improved aeroacoustic measurements. These data will be used to validate deterministic models that implement solutions to the wave equation within a cavity by imposing the constraints of the cavity geometry. Additionally, these data will support the development of models that use finite element methods and a lattice Boltzmann CFD simulations to analyze future cavity designs that further reduce TBL noise while improving the SNR of acoustic measurements.

Acknowledgement

The authors would like to thank the THAMES users group for their invaluable input.

Declaration of conflicting interests

The author(s) declared no potential conflicts of interest with respect to the research, authorship, and/or publication of this article.

Funding

The author(s) would like to thank The Netherlands Organization for Scientific Research (NWO) Applied and Engineering Sciences (TTW) domain for funding the THAMES project, NWO# 15215, of which this research is a part.

ORCID iD

Colin P VanDercreek https://orcid.org/0000-0003-2869-8124

References

1. Mueller TJ. *Experimental fluid mechanics: aeroacoustic measurements*. Berlin: Springer, 2002.
2. Kamruzzaman M, Lutz T, Würz W, et al. Validations and improvements of airfoil trailing edge noise prediction models using detailed experimental data. *Wind Energy* 2012; 15: 45–61.
3. Oerlemans S, Fisher M, Maeder T, et al. Reduction of wind turbine noise using optimized airfoils and trailing-edge serrations. *AIAA J* 2009; 47: 1470–1481.
4. Jaeger S, Horne W and Allen C. Effect of surface treatment on array microphone self-noise. In: *The 6th aeroacoustics conference and exhibit*, Aeroacoustics Conferences, 2000. Reston, VA: American Institute of Aeronautics and Astronautics.
5. Blake WK. *Mechanics of flow-induced sound and vibration*. 2nd ed. London: Academic Press, 2017.
6. Sijtsma P. *Phased array beamforming applied to wind tunnel and fly-over tests*. Report NLR-TP-2010-549, December 2010. Amsterdam: National Aerospace Laboratory NLR.
7. Sijtsma P. Clean based on spatial source coherence. *Int J Aeroacoust* 2007; 6: 357–374.
8. Merino Martinez R. *Microphone arrays for imaging of aerospace noise sources*. PhD Thesis, Delft University of Technology, Delft, The Netherlands, 2018.
9. Horne W and James K. *Concepts for reducing the self-noise of in-flow acoustic sensors and arrays*. Aeroacoustics Conferences, 1999. Reston, VA: American Institute of Aeronautics and Astronautics.
10. Fleury V, Coste L, Davy R, et al. Optimization of microphone array wall mountings in closed-section wind tunnels. *AIAA J* 2012; 50: 2325–2335.
11. DeLoach R. *Analysis of variance in the modern design of experiments*. Aerospace Sciences Meetings, 2010. Reston, VA: American Institute of Aeronautics and Astronautics.
12. Rienstra A and Hirschberg SW. *Fundamentals of duct acoustics*. Eindhoven: Eindhoven University of Technology, 2018.
13. Vandercreek CP, Sijtsma P, Snellen M, et al. Deterministic model of acoustic wave propagation in a cavity. In: *The 25th AIAA/CEAS aeroacoustics conference*, May 2019.
14. Goody M. Empirical spectral model of surface pressure fluctuations. *AIAA J* 2004; 42: 1788–1794.
15. De Jong AT. *Aeroacoustic resonance of slender cavities: an experimental and numerical investigation*. PhD Thesis, 2012.
16. Arguillat B, Ricot D, Robert G, et al. Measurements of the wavenumber-frequency spectrum of wall pressure fluctuations under turbulent flows. In: *The 11th AIAA/CEAS aeroacoustics conference*, Aeroacoustics Conferences, 2005. Reston, VA: American Institute of Aeronautics and Astronautics.
17. Montgomery DC. *Design and analysis of experiments*. 8th ed. Hoboken, NJ: John Wiley & Sons, Inc., 2013.
18. Landman D, Simpson J, Mariani R, et al. Hybrid design for aircraft wind-tunnel testing using response surface methodologies. *J Aircraft* 2007; 44: 1214–1221.
19. Morgan-Wall T and Khoury G. *skpr: Design of experiments suite: generate and evaluate optimal designs*. R package version 0.47.5, 2018.
20. Bruun HH. *Hot-wire anemometry: principles and signal analysis*. Oxford: Oxford University Press, 1995.
21. Nieuwstadt FTM, Westerweel J and Boersma BJ. *Turbulence: introduction to theory and applications of turbulent flows*. 1st ed., pp. 92–93. Berlin: Springer International Publishing, 2016.
22. Schoenherr KE. Resistance of flat surfaces moving through a fluid. *Trans SNAME* 1932; 40: 279–313.
23. Bates D, Mächler M, Bolker B, et al. Fitting linear mixed-effects models using lme4. *J Stat Soft* 2015; 67: 1–48.
24. Wood SN. *Generalized additive models: an introduction with R*. Boca Raton, FL: CRC Press, 2017.
25. Corcos GM. Resolution of pressure in turbulence. *J Acoust Soc Am* 1963; 35: 192–199.